Note: Dynamic strain field mapping with synchrotron X-ray digital image correlation

L. Lu, D. Fan, B. X. Bie, X. X. Ran, M. L. Qi, N. Parab, J. Z. Sun, H. J. Liao, M. C. Hudspeth, B. Claus, K. Fezzaa, T. Sun, W. Chen, X. L. Gong, and S. N. Luo

Citation: Review of Scientific Instruments **85**, 076101 (2014); doi: 10.1063/1.4887343
View online: http://dx.doi.org/10.1063/1.4887343
View Table of Contents: http://scitation.aip.org/content/aip/journal/rsi/85/7?ver=pdfcov
Published by the AIP Publishing

Articles you may be interested in
Optimization of in-line phase contrast particle image velocimetry using a laboratory x-ray source
J. Appl. Phys. **112**, 074701 (2012); 10.1063/1.4757407

Phase retrieval for improved three-dimensional velocimetry of dynamic x-ray blood speckle
Appl. Phys. Lett. **93**, 153901 (2008); 10.1063/1.3001592

True3D Strain Mapping for Assessment of Material Deformation by Synchrotron XRay Microtomography
AIP Conf. Proc. **760**, 1423 (2005); 10.1063/1.1916838

Fast CCD camera for x-ray photon correlation spectroscopy and time-resolved x-ray scattering and imaging
Rev. Sci. Instrum. **75**, 4383 (2004); 10.1063/1.1808913

Image observation of diffraction spots using FZP and coherent Xray beam
AIP Conf. Proc. **705**, 1332 (2004); 10.1063/1.1758047

This article is copyrighted as indicated in the article. Reuse of AIP content is subject to the terms at: http://scitationnew.aip.org/termsconditions. Downloaded to IP: 114.96.88.115 On: Wed, 16 Jul 2014 23:19:14

REVIEW OF SCIENTIFIC INSTRUMENTS **85**, 076101 (2014)

Note: Dynamic strain field mapping with synchrotron X-ray digital image correlation

L. Lu,[1,2] D. Fan,[2] B. X. Bie,[2,3] X. X. Ran,[3] M. L. Qi,[3,a)] N. Parab,[4] J. Z. Sun,[4] H. J. Liao,[4] M. C. Hudspeth,[4] B. Claus,[4] K. Fezzaa,[5] T. Sun,[5] W. Chen,[4,6] X. L. Gong,[1,b)] and S. N. Luo[2,c)]

[1]*CAS Key Laboratory of Mechanical Behavior and Design of Materials, Department of Modern Mechanics, University of Science and Technology of China, Hefei, Anhui 230027, People's Republic of China*
[2]*The Peac Institute of Multiscale Sciences, Chengdu, Sichuan 610207, People's Republic of China*
[3]*School of Science, Wuhan University of Technology, Wuhan, Hubei 430070, People's Republic of China*
[4]*School of Aeronautics and Astronautics, Purdue University, West Lafayette, Indiana 47907, USA*
[5]*Advanced Photon Source, Argonne National Laboratory, Argonne, Illinois 60439, USA*
[6]*School of Material Science Engineering, Purdue University, West Lafayette, Indiana 47907, USA*

(Received 24 May 2014; accepted 25 June 2014; published online 16 July 2014)

We present a dynamic strain field mapping method based on synchrotron X-ray digital image correlation (XDIC). Synchrotron X-ray sources are advantageous for imaging with exceptional spatial and temporal resolutions, and X-ray speckles can be produced either from surface roughness or internal inhomogeneities. Combining speckled X-ray imaging with DIC allows one to map strain fields with high resolutions. Based on experiments on void growth in Al and deformation of a granular material during Kolsky bar/gas gun loading at the Advanced Photon Source beamline 32ID, we demonstrate the feasibility of dynamic XDIC. XDIC is particularly useful for dynamic, in-volume, measurements on opaque materials under high strain-rate, large, deformation. *© 2014 AIP Publishing LLC.* [http://dx.doi.org/10.1063/1.4887343]

Optical techniques have contributed greatly to the field of dynamic materials science, but are mostly limited to surface measurements,[1,2] and the spatial and temporal resolutions achieved are not satisfactory in some cases. Diagnostics utilizing advanced synchrotron X-ray sources offer the promise of *in situ*, real time, in-volume measurements.[3,4] Recently, ultrafast and high-speed X-ray phase contrast imaging (XPCI) were demonstrated at the Advanced Photon Source (APS) beamline 32ID-B under gas gun and Kolsky bar loading,[5,6] for dynamic events with durations ranging from 100s ns to 100s μs, and strain rates from 10^2 s^{-1} to 10^6 s^{-1}. Such XPCI measurements can achieve a minimum exposure time of 100 ps and frame separation of 153 ns, as well as μm-level spatial resolution. Given recent advances in ultrafast/high speed X-ray imaging, development of corresponding data analysis and interpretation methods is desirable. Digital image correlation (DIC) has been established as an effective optical tool for full-field deformation measurement via tracking and image registration.[7–11] Furthermore, digital volume correlation (DVC) has been developed for three-dimensional strain mapping using quasi-static X-ray tomography,[12,13] which is an extension of two-dimensional (2D) DIC.

In this Note, we present a dynamic X-ray digital image correlation (XDIC) method, which is essentially a combination of ultrafast/high-speed X-ray PCI/radiography and DIC, and apply it to quantitatively mapping the strain fields during impact loading with Kolsky bars or gas guns. Two types of dynamic loading experiments are performed at APS to illustrate the XDIC methodology and its potential applications: Kolspky bar and gas gun loading. The experimental details were presented elsewhere.[5,6,14]

DIC requires artificial or inherent speckles for image correlation.[7,10] X-ray imaging is done in the transmission mode, and certain structural features (surface or internal) are needed to produce small-scale contrast, i.e., X-ray speckles, in the X-ray images. We use two types of Al samples, unetched and etched, and borosilicate glass beads, to explore the feasibility of dynamic XDIC with Kolsky bar and gas gun loading.

Chemical etching is a useful way to produce surface roughness which may give rise to X-ray speckles. For etching, a polished Al sample is first immersed in hydrofluoric acid for one minute, and then undergoes ultrasonic cleaning for half an hour to remove residual particles on the surfaces. The unetched and etched Al samples are characterized with XPCI and scanning electron microscope (SEM). The SEM images reveal more, although superficial, details than the X-ray images (Fig. 1). The X-ray image of the etched sample displays abundant artificial speckles due to the subtle difference in transmission thickness induced by chemical etching; this feature is more pronounced in the corresponding SEM image showing rich microstructure features. These X-ray speckles are similar to the optical speckles (e.g., via spray paint) obtained by laser diffuse scattering in optical DIC measurements. However, the unetched Al sample shows fair smoothness in both SEM and XPCI images.

In our proof-of-principles experiments, we prefabricate a through-hole with a diameter of about 100 μm in coarse-grained Al samples (grain size ∼ mm-level) using electrical discharge machining, in order to relate its growth dynamics with its strain fields. The Al samples are in a dog-bone

a)Electronic mail: qiml@whut.edu.cn
b)Electronic mail: gongxl@ustc.edu.cn
c)Electronic mail: sluo@pims.ac.cn

 © 2014 AIP Publishing LLC

This article is copyrighted as indicated in the article. Reuse of AIP content is subject to the terms at: http://scitationnew.aip.org/termsconditions. Downloaded to IP: 114.96.88.115 On: Wed, 16 Jul 2014 23:19:14

FIG. 1. XPCI (a) and SEM (b) images of etched Al.

shape with a thickness of about 0.5 mm. The void is located in the center of the experimental section, across the whole thickness, and subjected to the Kolsky tension bar loading at the APS beamline 32ID-B.[6] During dynamic loading, the X-ray speckles remain evident for the etched Al sample (Fig. 2) but are absent for the unetched one.

In XDIC analysis, we take two consecutive images in an image sequence, the reference and current images, to perform 2D image correlation, and calculate the displacement vectors, U_k, and the Green-Lagrange strain tensor, E_{kl} ($k, l = 1, 2$).[7–11] We divide both images equally into subsets (S) of an appropriate size. For a subset in the reference frame and another one in the current frame, the correlation coefficient based on the normalized least-square criterion is

$$C(S, \tilde{S}) = \sum_{(i,j)\in S,\tilde{S}} \left\{ \frac{f(x_i, y_j) - f_{\mathrm{m}}}{\sqrt{\sum_{(i,j)\in S}[f(x_i, y_j) - f_{\mathrm{m}}]^2}} - \frac{\tilde{f}(\tilde{x}_i, \tilde{y}_j) - \tilde{f}_{\mathrm{m}}}{\sqrt{\sum_{(i,j)\in \tilde{S}}[\tilde{f}(\tilde{x}_i, \tilde{y}_j) - \tilde{f}_{\mathrm{m}}]^2}} \right\}^2, \quad (1)$$

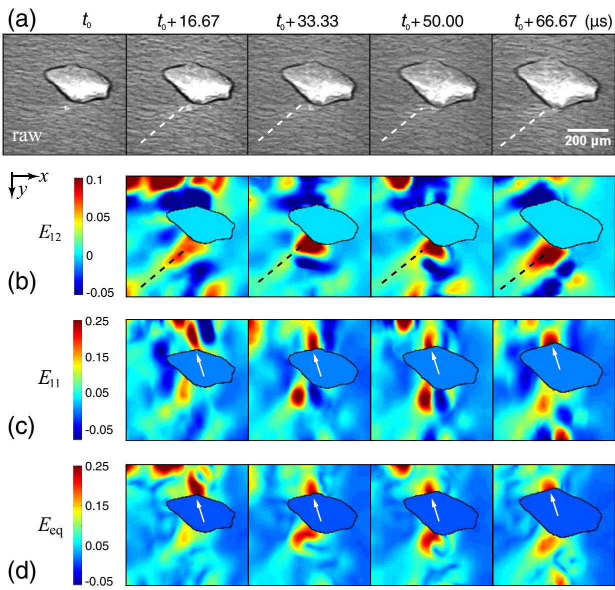

FIG. 2. (a) PCI image sequence of etched Al stretched along the x-direction under Kolsky tension bar loading, and corresponding XDIC results: E_{12} (b), E_{11} (c), and E_{eq} (d). The voids are outlined (black curves) on the strain maps. t_0 denotes the reference frame.

where the first term in the curly brackets refers to the reference frame, and the second term, the current frame (denoted with accent tilde); x and y are coordinates; f is the grayscale value function, and subscript m denotes the mean grayscale value. $C(S, \tilde{S})$ quantifies the degree of match between S and $\tilde{S}$, and it is zero for a good match.[10] After the correspondence between the subsets is established, the displacement field U_k and strain field E_{kl} can be obtained, including the von Mises equivalent strain (E_{eq}).

The etched Al sample is stretched at a bar velocity of ~8 m s^{-1}, and some representative, dynamic, XPCI images are shown in Fig. 2(a). Visual observation reveals deformation and growth of the void under increasing tension, as well as vague shear bands as indicated by the dotted lines. The shear strain E_{12} obtained from the XDIC analysis shows marked shear banding extending from the lower corner of the void to the lower edge [Fig. 2(b)]. The shear strain is concentrated around the two corners of the void, in particular the lower one, and increases with increasing time; normal strain E_{11} and von Mises strain E_{eq} are also much higher in these regions [Figs. 2(c) and 2(d)]. As a result, fracture occurs near the upper corner along the y-axis in the absence of shear banding but with appreciable normal tensile strain E_{11}, while fracture near the lower corner develops along the shear band; therefore, two damage modes, mode I crack vs. shear banding, are observed. The von Mises equivalent shear strain E_{eq} reflects the degree of local plastic deformation; growth of the void is achieved via pronounced plastic deformation around the top and bottom corners of the void, and shear banding is also accompanied by plasticity [Fig. 2(d)].

In addition, we estimate the noise level by correlating two images captured at different instants before dynamic loading. The result shows the noise level in strain is minor, on the order of 10^{-3}. Uncertainty is also calculated in a way similar to Bornert *et al.*[15] In our estimation, we simply take the first image in Fig. 2(a), and deform it with an elongation along the X_1-direction by 25%. The original and deformed images are used for DIC analysis, which yields the Green-Lagrange strain $E_{11} = 0.2804 \pm 0.0039$, with 1%–2% uncertainty. Given $\partial U_1/\partial X_1 = 0.25$, $\partial U_2/\partial X_1 = 0$, we calculate the theoretical $E_{11} = 0.2813$, in excellent agreement with the XDIC analysis. These calculations indicate that the noise level and uncertainty in our XDIC analyses are reasonable.

The strain field maps show excellent correlation with the dynamics of void growth and fracture as well as shear banding in the case of the etched Al sample. However, the X-ray speckles are missing in the raw images for the unetched Al under similar loading conditions. The contrast between unetched and etched Al highlights the importance of X-ray speckles for a useful XDIC analysis. X-ray speckles could be produced during deformation in principle, but it is certainly ineffective for the unetched Al. A minimum surface roughness, as those on the etched Al surfaces, is required to produce X-ray speckles.

Dynamic XDIC strain field mapping with ultrafast imaging (a minimum 100-ps exposure time and 153-ns frame separation currently available at APS)[5] is also of interest for extreme conditions such as gas gun loading. In addition to surface roughness, internal inhomogeneities can be exploited

This article is copyrighted as indicated in the article. Reuse of AIP content is subject to the terms at: http://scitationnew.aip.org/termsconditions. Downloaded to IP: 114.96.88.115 On: Wed, 16 Jul 2014 23:19:14

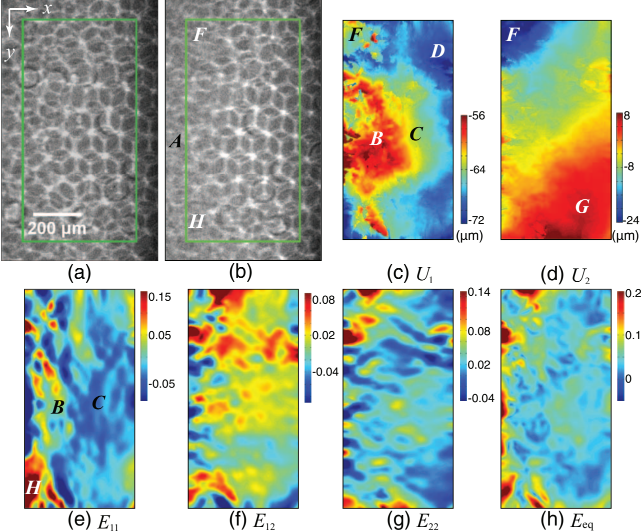

FIG. 3. Preshock (a) and dynamic (b) XPCI images of borosilicate glass beads impacted along the *x*-axis, along with XDIC results of the selected region indicated by the rectangles in (a) and (b), including U_1 (c), U_2 (d), E_{11} (e), E_{12} (f), E_{22} (g), and E_{eq} (h). (a) and (b) are modified from Ref. 5.

to produce X-ray speckles. We perform XDIC analysis of borosilicate glass beads embedded in polymethyl methacrylate (PMMA) plates impacted by a gas gun-launched flyer plate.[5] The diameter of the glass beads is about 106 μm. The raw images in Figs. 3(a) and 3(b) suggest that the granular microstructure due to the glass beads can serve as X-ray speckles.

The XDIC analysis yields the displacement and strain fields within a selected area [Figs. 3(c)–3(h)]. The horizontal displacements are all negative, i.e., $U_1 < 0$, because of the recoil of the gun barrel during firing. The displacement field U_1 is highly inhomogeneous, showing distinct regions $B - D$ and F. The upward movement in region F and downward movement in G are due to the forward movement in regions B and C. Region C represents a compressional "precursor," while region B undergoes partial expansion as indicated by E_{11} [Fig. 3(e)]. Shear strain field E_{12} is nonuniform, with an appreciable concentration in the junction area of regions $B - D$ and F [Fig. 3(f)]. E_{22} and E_{eq} show spatial variations consistent with the inhomogeneity of granular materials [Figs. 3(g) and 3(h)]. Region A is not appropriate for XDIC because of the crushed beads. Thus, the granular material experiments validate ultrafast XDIC with inherent markers, but also underscore the importance of preserving the integrity of X-ray speckles (the crushing induces the loss of correlating speckles).

In summary, we have established the feasibility of XDIC for high strain-rate, large deformation, dynamic loading with Kolsky bar and gas gun experiments on bulk and granular materials, and XDIC can be extended to other dynamic processes. XDIC requires surface or interior structure inhomogeneities to produce X-ray speckles, and such microstructures can be engineered or inherent (e.g., particle-reinforced composites). With properly structured X-ray pulses (in time) as supplied by a synchrotron, high quality image sequences can be obtained for XDIC. XDIC has its unique advantages and is a useful complement to optical DIC. For example, it is difficult to apply optical DIC to certain cases of granular materials, interiors of opaque materials, severely deformed spray speckles, weak return of scattered light, and short exposure time and frame separation. X-ray images supply extra information on interior deformation besides the strain fields from XDIC. Therefore, XDIC provides opportunities for exploring materials and processes previously not promised by conventional optical DIC. By utilizing synchrotron X-ray sources, diffraction and imaging can be performed simultaneously.

This work was supported in part by the National Natural Science Foundation of China (NNSFC) and NSAF (Grant Nos. 11172221 and U1330111). Use of the Advanced Photon Source, an Office of Science User Facility operated for the (U.S.) Department of Energy (DOE) Office of Science by Argonne National Laboratory, was supported by the (U.S.) DOE under Contract No. DE-AC02-06CH11357.

[1] L. M. Barker and R. E. Hollenbach, J. Appl. Phys. **43**, 4669 (1972).
[2] D. L. Paisley, S. N. Luo, S. R. Greenfield, and A. C. Koskelo, Rev. Sci. Instrum. **79**, 023902 (2008).
[3] B. M. Ocko, J. Wang, A. Davenport, and H. Isaacs, Phys. Rev. Lett. **65**, 1466 (1990).
[4] E. Pagot, P. Cloetens, S. Fiedler, A. Bravin, P. Coan, J. Baruchel, J. Hartwig, and W. Thomlinson, Appl. Phys. Lett. **82**, 3421 (2003).
[5] S. N. Luo, B. J. Jensen, D. E. Hooks, K. Fezzaa, K. J. Ramos, J. D. Yeager, K. Kwiatkowski, and T. Shimada, Rev. Sci. Instrum. **83**, 073903 (2012).
[6] M. Hudspeth, B. Claus, S. Dubelman, J. Black, A. Mondal, N. Parab, C. Funnell, F. Hai, M. L. Qi, K. Fezzaa, S. N. Luo, and W. Chen, Rev. Sci. Instrum. **84**, 025102 (2013).
[7] T. C. Chu, W. F. Ranson, and M. A. Sutton, Exp. Mech. **25**, 232 (1985).
[8] M. A. Sutton, M. Q. Cheng, W. H. Peters, Y. J. Chao, and S. R. McNeill, Image Vis. Comput. **4**, 143 (1986).
[9] H. A. Bruck, S. R. McNeill, M. A. Sutton, and W. H. Peters III, Exp. Mech. **29**, 261 (1989).
[10] B. Pan, K. Qian, H. Xie, and A. Asundi, Meas. Sci. Technol. **20**, 062001 (2009).
[11] B. Pan, Appl. Opt. **48**, 1535 (2009).
[12] B. K. Bay, T. S. Smith, D. P. Fyhrie, and M. Saad, Exp. Mech. **39**, 217 (1999).
[13] N. Lenoir, M. Bornert, J. Desrues, P. Bésuelle, and G. Viggiani, Strain **43**, 193 (2007).
[14] W. W. Chen, M. C. Hudspeth, B. Claus, N. D. Parab, J. T. Black, K. Fezzaa, and S. N. Luo, Philos. Trans. R. Soc. London, Ser. A **372**, 20130191 (2014).
[15] M. Bornert, F. Brémand, P. Doumalin, J. C. Dupré, M. Fazzini, M. Grédiac, F. Hild, S. Mistou, J. Molimard, J. J. Orteu, L. Robert, Y. Surrel, P. Vacher, and B. Wattrisse, Exp. Mech. **49**, 353 (2009).

This article is copyrighted as indicated in the article. Reuse of AIP content is subject to the terms at: http://scitationnew.aip.org/termsconditions. Downloaded to IP: 114.96.88.115 On: Wed, 16 Jul 2014 23:19:14